Chinese Chemical Letters 32 (2021) 3231–3236

Contents lists available at ScienceDirect

Chinese Chemical Letters

journal homepage: www.elsevier.com/locate/cclet

Communication

Synthesis of Mg(II) doped ferrihydrite-humic acid coprecipitation and its Pb(II)/Cd(II) ion sorption mechanism

Jing Li, Zhuanjun Zhao*, Yiran Song, Yang You, Jie Li, Xiuwen Cheng*

Key Laboratory of Western China's Environmental Systems (Ministry of Education) and Key Laboratory for Environmental Pollution Prediction and Control, Gansu Province, College of Earth and Environmental Sciences, Lanzhou University, Lanzhou 730000, China

ARTICLE INFO

Article history:
Received 3 December 2020
Received in revised form 27 February 2021
Accepted 30 March 2021
Available online 2 April 2021

Keywords:
Ferrihydrite
Humic acid
Magnesium
Adsorption

ABSTRACT

A magnesium doped ferrihydrite-humic acid coprecipitation (Mg-doped Fh-HA) was synthesized by coprecipitation method. The removal of heavy metals such as Pb(II) and Cd(II) was assessed. The isotherms and kinetic studies indicated that the Mg-doped Fh-HA exhibited a remarkable Pb(II) and Cd(II) sorption capacity (maximum 120.43 mg/g and 27.7 mg/g, respectively.) in aqueous solution. The sorption of Pb(II) and Cd(II) onto best fitted *pseudo*-second-order kinetic equation and Langmuir model. The adsorption mechanism of Mg-doped Fh-HA on Pb(II) and Cd(II) involves surface adsorption, surface complexation and surface functional groups (such as carboxyl group, hydroxyl group). In addition, ion-exchange and precipitation cannot be ignored. The Mg-doped Fh-HA is a low-cost and high-performance adsorption material and has a wide range of application prospects.

Lead (Pb) and cadmium (Cd) pollution widely exists in the water environment and cause significant harm to human health. Lead is shown to induce changes in the composition of red blood cell (RBC) membrane proteins and lipids [1] and inhibit hemoglobin synthesis [2]. The binding of cadmium to proteins containing hydroxyl, amino and sulfhydryl groups can inhibit many enzyme systems, thus affecting the normal function of enzyme systems in liver and kidney organs [3]. However, the elimination of metal ions from industrial wastewaters remains problematic. Ferrihydrite is a poorly crystalline Fe(III) oxyhydroxide, common in soils and sediments [4]. Owing to its high surface area and intrinsic reactivity [5]. Humic acid (HA) exits in environment widely. The humic acid has high activity and is easy to interact with the natural mineral particles and metal ions. Though it has been found that HA components compete for adsorption sites with target ions during the adsorption [6], few scholars pay close attention to the adsorption ability of ferrihydrite-humic acid (Fh-HA) complex doped with ions. The interaction between soil organic matter and iron oxide is an important factor controlling the stability of soil organic carbon [7].

Unlike organic pollutants which could be bio-degraded or chemically oxidized, metal ions could not be degraded. Adsorption is widely used in industrial manufacture [8]. A large number of studies have shown that there are many active groups in the adsorbents, such as hydroxyl, carboxyl, amino groups and aromatic groups [9]. These groups adsorb metal ions by forming electrovalent bonds or covalent bonds with metal ions. It is the most cost-effective method based on investment costs, energy consumption, throughput capacity, and toxic by-products generation. Mesoporous materials have the advantages of large specific surfaces, orderly pore structure, strong adsorption properties and high stability [10]. Adsorbed and precipitated organic matter decreases the SSA by blocking surface sites on the ferrihydrite surfaces and initiating aggregation [11,12]. Doping of ions is considered as a feasible way to improve the reaction activity of the material. The surface and structural properties of iron oxides can be modified by doping metal ions into the iron matrix [13]. In particular, the doping of Mg ions can more available enhances the adsorption property of the Fe-C co-precipitation. Magnesium (Mg) is one of the most abundant alkaline-earth metal ions in nature and interaction with ferrihydrite (Fh) affects the geochemical cycle of substances, including HA. Although the Fh-HA co-precipitation is very active and selective, they have some disadvantages: (i) The Fh-HA co-precipitation is difficult to recover and utilize in soil environment. (ii) The active oxidation state is unstable, partial ferrihydrite will be converted into hematite and goethite. (iii) In soils, Mg^{2+} ions are mostly adsorbed at surfaces/interlayers ("exchangeable Mg") and incorporated into the crystal structures ("structural Mg") of clay minerals and Fe/Mn oxides. Besides, Mg^{2+}

* Corresponding authors.
E-mail addresses: zhj_zhao@lzu.edu.cn (Z. Zhao), chengxw@lzu.edu.cn (X. Cheng).

https://doi.org/10.1016/j.cclet.2021.03.086
1001-8417/

ions can be complexed by organic matter because Mg^{2+} ions with light Mg isotopes from soil waters could be incorporated into the crystal structures of secondary mineral neoformation. This study enables the use of Mg as a representative of alkaline-earth metals, which will contribute to an improved understanding of the mutual interaction of iron oxides with humic acid complexes with M^{2+} in natural systems. To this aim instrumental analysis is combined with experimental results. The findings from this study have important implications for understanding Pb and Cd mobility and bioavailability in Pb/Cd-contaminated reducing environmental settings.

The surface morphology and chemical composition of Fh-HA and Mg-doped Fh-HA were characterized using scanning electron microscope (SEM), and typical images are given in Figs. 1a and b. The surface of Fh-HA was smooth and irregular as seen in Fig. 1a. As shown in Fig. 1b, the Mg-doped Fh-HA was loose, coarse, vary in size and crevices. The surface of Mg-doped Fh-HA looked much rougher compared with Fh-HA which meant that the adsorption effect of the Mg-doped Fh-HA is better. Moreover, The energy-dispersive X-ray spectroscopy (EDX) of the adsorbed Pb(II) and Cd (II) were shown in Figs. 1c and d. It also indicated that the presence of C, O, Fe and Mg in the Mg-doped Fh-HA.

In general, surface of the humic acid has a large amount of negative charge, which can reduce the aggregation and deposition of the particles by electrostatic and steric hindrance effect [14]. Combined with the pore size distribution map, the adsorbents have a high mesoporous structure. Brunauer-Emmett-Teller (BET) of Mg-doped Fh-HA was displayed in Fig. S1 (Supporting information). The typical type IV isotherms with a H3-type hysteresis loops of all samples suggested the slit-shaped meso-porous in the Mg-doped Fh-HA and the possibility of capillary condensation in the pores [15]. The specific surface area and average pore width of the Mg-doped Fh-HA are 145.3 m^2/g and 2.3 nm, respectively. Compared with Fh-HA, the specific surface area and average pore width less change. They are 183.1 m^2/g and 2.01 nm, respectively. The specific surface area of the iron oxide is large, with a positive charge, which can be exchanged with a negatively charged humic acid molecule. This suggests that humic acid may occupy part of the surface of iron oxide to a certain extent, thus affecting the adsorption of heavy metals. When the Mg(II) is doped, the specific surface area change is small, which indicates that the doping of the magnesium does not occupy the adsorption site of the co-precipitate surface. Other sorbent parameters are listed in Table S1 (Supporting information) for comparison.

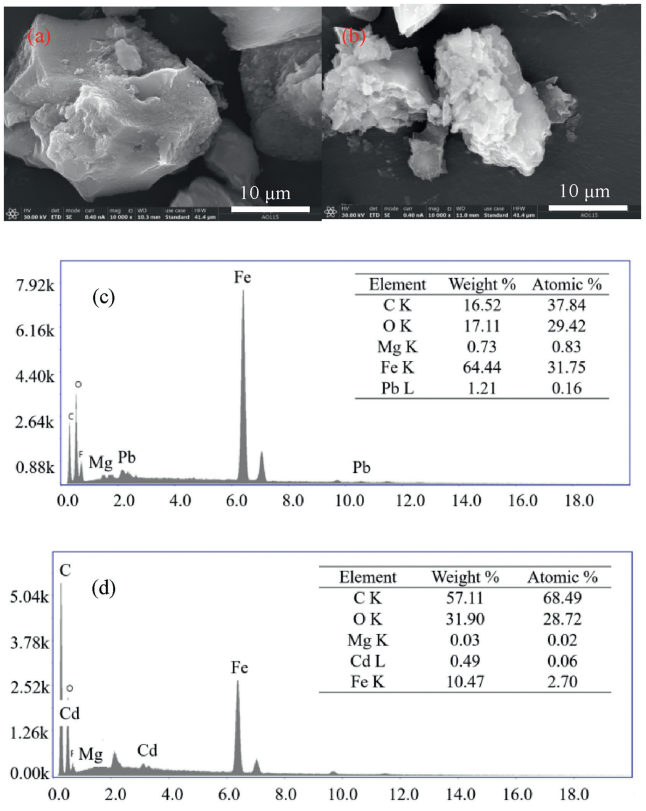

Fig. 1. SEM image of Fh-HA (a), Mg-doped Fh-HA (b). The EDX images of Mg-doped Fh-HA adsorbed Pb(II) (c), Mg-doped Fh-HA adsorbed Cd(II) (d).

To analyze the crystalline phase of Mg-doped Fh-HA, the X-ray diffraction (XRD) patterns of Mg-doped Fh-HA was presented in Fig. S2 (Supporting information). Fig. S2 shows the presence of 2-line ferrihydrite phase in all the metal loaded samples. The XRD patterns of metal ion loaded samples indicated that during adsorption the relative intensities alter. No visible peaks from other phases were observed, revealing the high purity of the Mg-doped Fh-HA nano composite [16]. Compared with Fh-HA, the crystallization of Mg-doped samples became better before and after adsorption of heavy metal ions. No appearance of other phases may be due to due to the small amount of magnesium doping. The migration phenomenon before and after adsorption indicates that —OH and —COOH functional groups play an essential role in the adsorption process of Pb(II) and Cd(II) [17].

The speciation distribution of heavy metals in aqueous solution has a great influence on the adsorption efficiency of heavy metals. The pH of the solution is also an important factor in the absorption process [18]. The adsorption efficiency of Pb(II) and Cd(II) on the Mg-doped Fh-HA at the wide pH values ranging from 3.0 to 10.0 is shown in Fig. 2a. the adsorption amounts for both Pb(II) and Cd(II) were obviously increased at $pH > 6$ and $pH > 5$, respectively. Affecting the metal ion species, the diffuse double layer of solid-liquid interface and the adsorption process [19]. For example, cadmium and lead mainly exist as the cationic Cd(II) and Pb(II) at lower pH and forms a precipitate at higher pH. The adsorption capacity of Mg-doped Fh-HA precipitate for Pb(II) and Cd(II) varies obviously with the change of pH. For Pb(II), when solution pH is greater than or equal to 6, the adsorption is basically in equilibrium. However, Cd(II) is different. Ion exchange and surface coordination play an important role when $pH > 6$, because the deprotonating of the surface groups of the Mg-doped Fh-HA is enhanced. But when $pH < 4$, the protonation reaction mainly occurs on the surface site. Acid dissolution affects the adsorption of heavy metal ions on the surface. Under low pH conditions, competitive adsorption of H^+ and Pb(II)/Cd(II) resulted in lower adsorption rates. Under neutral and basic conditions, such protonation is inhibited and thus pH does not exert significant influence on the adsorption capacity [20].

The ionic strength in the solution affects the interfacial potential of the adsorbents and the thickness of the diffusion double layer [21]. The different ionic strengths, such as 0, 0.005, 0.01, 0.05, 0.1 and 0.2 mol/L NO_3^- were chosen to investigate their effect on Pb(II) and Cd(II) ion adsorption by Mg-doped Fh-HA. Fig. 2b shows that Cd(II) ion adsorption decreases and Pb(II) ion adsorption increases with increasing NO_3^- concentration. This phenomenon could be attributed to following reasons: The Cd(II) ion probably forms outer-sphere complexes with the adsorbent sites, which favor the adsorption when the concentration of the competing salt is decreased. This might indicate that ionic strength of solution influences the activity coefficient of metal ions, which limits their transfer to the composite surfaces. However, ionic strength showed positive effect on Pb(II) adsorption to Mg-doped Fh-HA, adsorption of Pb(II) on Mg-doped Fh-HA sample increased with increasing ionic strength of the background electrolyte. This is because there is a chemical bond with coordination covalent bond

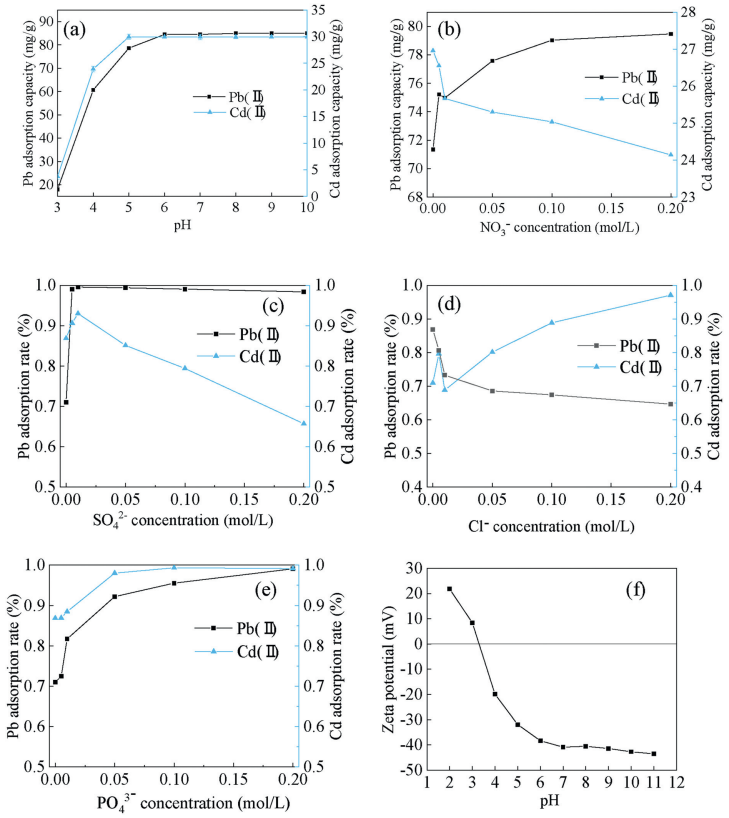

Fig. 2. Effect of pH (a), ionic strength (b-e) and on the adsorption efficiency of Pb(II) and Cd(II) by Mg-doped Fh-HA. Zeta-potential of Mg-doped Fh-HA as a function of pH (T =293 K) (f).

between Pb(II) and Mg-doped Fh-HA, which forms the inner layer surface complex, which is beneficial to the movement and interaction of other ions in the solution. Play a certain catalytic role [22]. In addition, the effects of SO_4^{2-}, Cl^-, PO_4^{3-} on Pb(II) and Cd(II) ion adsorption by Mg-doped Fh-HA were studied. The adsorption efficiency of Pb(II) and Cd(II) on the Mg-doped Fh-HA at different ionic strength is shown in Figs. 2c-e. The effect of Cl^- the same as NO_3^-. With the increase of ionic strength, humic acid is compressed because of electrostatic action and the surface actively sites of ferrihydrite increases, there is a weak "bridge" action. When adsorption efficiency decreases with the increase of ionic strength, an outer surface complexation may be formed between Cd(II) and the Mg-doped Fh-HA. Because of a lot of Na^+, cation repulsion also hinders the combination of Cd(II) and the Mg-doped Fh-HA. The addition of PO_4^{3-} also promoted the adsorption of Pb(II) and Cd(II), mainly because PO_4^{3-} can bind to Pb^{2+} and Cd^{2+} to form insoluble phosphate substances, thus stabilizing them in the form of precipitation.

The zeta potential of Mg-doped Fh-HA was measured in the pH range of 2.0–11.0, and the results are shown in Fig. 2f. The zeta potentials of Mg-doped Fh-HA was found to be negative over the entire environmentally relevant pH range, and gradually becomes negative with the increase of solution pH and then tends to be gentle, indicating that there are enough negative charges on the surface of the modified Mg-doped Fh-HA to attract and adsorb with positively charged metal ions. Given the fact that the outer sphere species does not affect the surface charge [22], this observation suggests that Pb(II) adsorbs to Mg-doped Fh-HA through the formation of an inner sphere surface complex, consistent with the results of the ionic strength analyses.

Effect of contact time on the Pb(II) and Cd(II) adsorption capacities by the Mg-doped Fh-HA is shown in Fig. S3a (Supporting information). As can be seen from Fig. S3a, both the Pb(II) and Cd(II) adsorption capacity increased with the adsorption time increasing, and then achieved adsorption equilibrium. In the beginning of fast adsorption, it may be explained due to the availability of more number of adsorption sites [23,24]. Through the study of contact time of the Mg-doped Fh-HA adsorption of Pb(II) and Cd(II). The fitting plots of *pseudo*-first-order and *pseudo*-second-order kinetic models and the corresponding parameters of the two models are collected in Figs. S3b-e and Table S2 (Supporting information). According to Figs. S3b-e and Table S2, the adsorption kinetic for both Pb(II) and Cd(II) can be depicted by *pseudo*-second-order kinetic model. The correlation coefficient R^2 of *pseudo*-first-order kinetics of Pb(II) is 0.984, and the equilibrium adsorption capacity q_e =24.29 mg/g, is quite different from that of the experiment. The correlation coefficient of *pseudo*-second-order kinetics is R^2 = 0.996, and the equilibrium adsorption capacity q_e = 71.43 mg/g, is close to the experimental data. The correlation coefficient R^2 of *pseudo*-first-order kinetics of Cd is 0.964, and the equilibrium adsorption capacity q_e = 12.8 mg/g, is quite different from that of the experiment. The correlation coefficient of *pseudo*-second-order kinetics is R^2 = 0.994, and the equilibrium adsorption capacity q_e = 27.77 mg/g, is in great agreement with the experimental results. This indicates that the adsorption of the Mg-doped Fh-HA is in accordance with the *pseudo*-second-order kinetic model. It also shows that the adsorption process is chemical adsorption and controlled by chemical adsorption mechanism [25]. The *k*-value of Pb(II) is greater than that of Cd(II), which indicates that the adsorption of the former is faster.

Freundlich adsorption isotherms and Langmuir adsorption isotherms were used to fit them respectively, and the equations were as follows, where Eqs. 1 and 2 are Freundlich and Langumuir linearized equations, respectively,

$$\log q_e = \log K_F + 1/n \log C_e \quad (1)$$

$$C_e/q_e = (1/q_m)\ b + C_e/q_m \quad (2)$$

Where q_e is the equilibrium adsorption capacity (mg/g), C_e is the equilibrium concentration (mg/L), q_m is the maximum adsorption capacity (mg/g) for Langmuir isotherms. b is a constant related to adsorption heat. K_F and n were the Freundlich constants, which represented the adsorption capacity and the adsorption strength, respectively. $1/n$ shows the effect of concentration on adsorption capacity. The smaller the $1/n$, the better the adsorption performance. K_F decreases with the increase of temperature. The experiment was carried out at room temperature.

Generally speaking, the description of adsorption phenomenon cannot be separated from adsorption capacity, adsorption strength and adsorption state and so on. The linear fitting data of Pb(II) and Cd(II) adsorption by Mg-doped Fh-HA are shown in Table S3 (Supporting information). Compared to the Freundlich model, the Langmuir model showed R^2 of 0.981 and 0.998 for Pb and Cd, respectively. q_m is 120 mg/g and 27.77 mg/g, respectively. The q_m obtained from Langmuir model is closer to the experiment data, further suggesting Langmuir model is appropriate to describe the adsorption process. These results showed that the adsorption efficiency of Pb(II) and Cd(II) was closely related to the number of active adsorption sites. This also demonstrates the adsorption of Pb (II) and Cd(II) is proceeded by monolayer adsorption behavior [23].

Thermodynamic parameters provide additional in-depth information regarding the inherent energetic changes involved during adsorption. To assess the thermodynamic parameters, the adsorption isotherm of Pb(II) and Cd(II) ions onto Mg-doped Fh-HA surfaces were measured at 283, 293 and 303 K, and the changes in thermodynamic parameters of standard Gibbs free energy of adsorption (ΔG^0), standard enthalpy (ΔH^0) and standard entropy (ΔS^0) were calculated from the thermodynamic equation, as follows (Eqs. 3–5):

$$K_d = \frac{q_e}{C_e} \quad (3)$$

$$\Delta G^0 = -\mathrm{RT}\ln K_d \quad (4)$$

$$\ln K_d = \frac{\Delta H^0}{RT} + \frac{\Delta S^0}{R} \quad (5)$$

where q_e is the concentration of ion adsorbed onto the surface (mg/g), C_e is the concentration of considered ion at the equilibrium (mg/L), R, T, K_d are the universal gas constant (8.314 J mol^{-1} K^{-1}), the temperature in Kelvin, and the distribution coefficient, respectively.

The values of ΔG^0 and K_d are calculated at 10, 20 and 30 °C, respectively, and the results are shown in Table S4 (Supporting information). Linear plots of ln K_d versus 1/T for the adsorption of Pb(II) and Cd(II) on different serpentines at 10, 20 and 30 °C are given in Fig. S4 (Supporting information). By fitting each linear, the values of ΔS^0 and ΔH^0 are estimated, as shown in Table S4. ΔG^0 is negative at different adsorption temperatures for all samples, indicating that the adsorption of Pb(II) and Cd(II) on the Mg-doped Fh-HA is a spontaneous process. And the absolute value of ΔG^0 increases with the increase of adsorption temperature, which demonstrates that increasing temperature can increase the spontaneity of adsorption. The positiveΔH^0 value for Mg-doped Fh-HA suggests that the adsorption process is endothermic, and a proper increase of the temperature is beneficial to the adsorption. The positive ΔS^0 value for Mg-doped Fh-HA indicates that the adsorption of Pb(II) and Cd(II) on solid-liquid interface of Mg-doped Fh-HA is disordered and together with greater confusion.

The FTIR spectra of Fh-HA, Mg-doped Fh-HA, loaded Pb and loaded Cd samples are shown in Fig. 3, the broad band around 3362.4 cm^{-1} can be attributed to —OH group stretching vibration. The broad adsorption peaks around 1565.7 and 1368.7 cm^{-1} represent the stretching vibrations of C=C and carboxyl C=O [26]. The band at 1039 cm^{-1} is attributed to C—O stretching vibrations [27], but it shift to 1037.2 and 1035.6 cm^{-1} for loaded Pb and loaded Cd, respectively. The peak at 910.6 cm^{-1} was attributed to M—O bond or M—O—M mode stretching vibrations due to the influence of electrostatic interaction [28]. In addition, it noted that a band at 426.6 cm^{-1} might be partly attributed to Fe_3O_4 Fe–O stretching vibration peaks [29]. The primary adsorption bond at around 1383.9 cm^{-1} was assigned –NO_2 symmetric stretching vibration, and also the peak obtained 1110.6 cm^{-1} could be associated with C—O stretching vibration [30]. It indicated that the hydroxyl and the carboxyl groups are involved in the adsorption reaction to form inner complexes (—COOM, —OM and Fe—OM (M = Pb or Cd)) [31]. Peak at 2921.7 cm^{-1} is for asymmetrical C—H stretching of methylene group. The band at 1328.2 cm^{-1} was shifted to 1368.7 cm^{-1} in all the Mg-doped samples. Besides, these spectra provided proof for existence between Fh-HA and Mg(II) [31]. Combined with XRD analysis, it is shown that the main reason for the efficient adsorption of Pb(II) and Cd(II) by Mg-doped Fh-HA co-precipitates is the complexation of surface functional groups.

In order to further investigate the removal mechanism of Pb(II) and Cd(II) by Mg-doped Fh-HA, the X-ray photoelectron spectroscopy (XPS) measurements and the relevant results are illustrated in Fig. 4. The surface composition of Mg-doped Fh-HA co-precipitates contains C, O, Fe and Mg. The significant peaks corresponding to Pb 4f, Pb 4d and Cd 3d were observed on Mg-doped Fh-HA after Pb(II) and Cd(II) were absorbed. These illustrate Pb(II) are adsorbed on the co-substrate in many ways. Therefore, the XPS analysis result further explains that Pb(II) and Cd(II) may be ion-exchange with the Mg—O and Fe—OH functional groups of Mg-doped Fh-HA [18]. The main functional groups were characterized using high-resolution XPS spectra of C 1s. Before and after Pb(II) and Cd(II) adsorption C 1s peaks hardly changed. The peaks centered at 136.8 eV and 141.7 eV can be assigned to Pb $4f_{7/2}$ and Pb

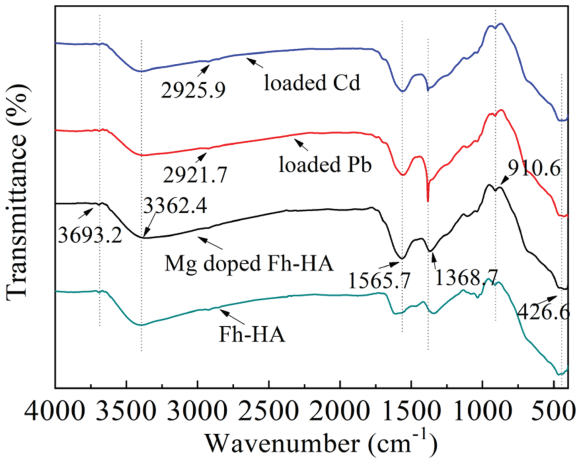

Fig. 3. The FT-IR spectra of Mg-doped Fh-HA before and after loading metal.

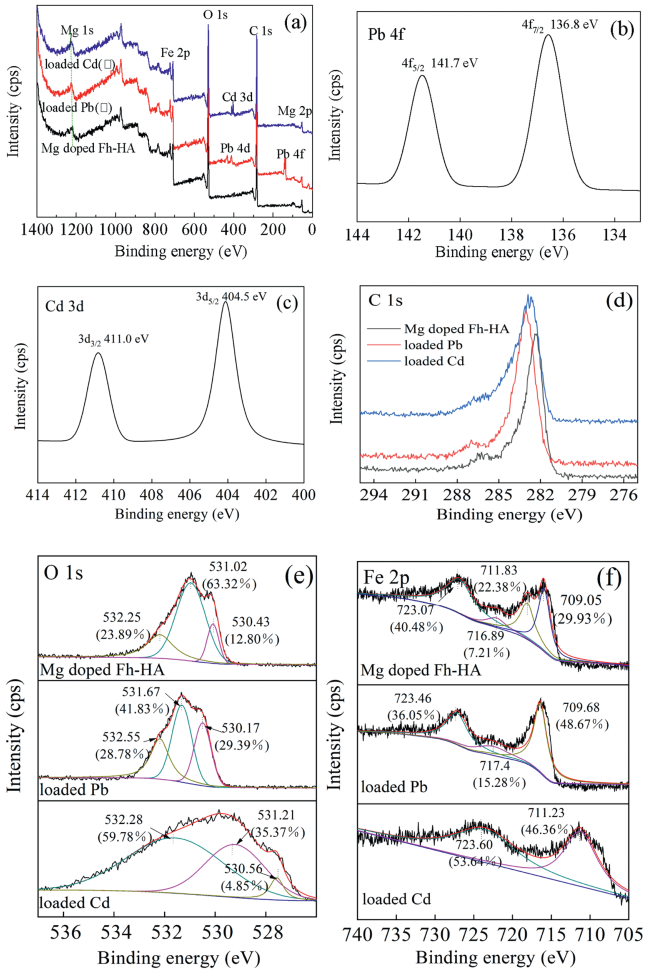

Fig. 4. XPS spectra of Mg-doped Fh-HA before and after adsorption for Pb(II) and Cd (II) (a), Pb 4f (b), Cd 3d (c), C 1s (d), O 1s (e), Fe 2p (f) energy regions.

$4f_{5/2}$, respectively. Demonstrating the presence of Pb(II) in the adsorbed samples. Binding energy of Cd $3d_{5/2}$ and Cd $3d_{3/2}$ appears at 404.5 eV and 409.8 eV, respectively. This result further confirms that the Pb(II) and Cd(II) is adsorbed on the nanostructured Mg-doped Fh-HA.

The O 1s spectrum (Fig. 4e) was deconvoluted into three peaks, located at 532.25, 531.02 and 530.43 eV, which can be ascribed to C—O/C—O—C, FeOOH/O—H and C=O, respectively [32].We discovered the ratio of C—O/C—O—C peak areas grown after Pb(II) (23.89%–28.78%) and Cd(II) (23.89%–59.78%) adsorption. Meanwhile, the ratio of C=O peak areas increased from 12.80% to 29.39% after adsorption of Pb(II). However, the ratio of FeOOH/O—H peak areas decreased from 63.32%–41.83% or 35.37% after adsorption of Pb(II) or Cd(II), respectively. The prominent reduction of oxygen for C—OH/FeOOH indicates that hydroxyl and carboxyl groups of Mg-doped Fh-HA surely participate in the adsorption process. These results suggest that there is a strong complexation between Pb(II), Cd(II) and Mg-doped Fh-HA as well as oxygen-containing functional groups on Mg-doped Fh-HA, and the complexation played a vital role in the removal process of Pb(II) and Cd(II) by Mg-doped Fh-HA. In addition, the role of the ion exchange reaction and microporous adsorption cannot be ignored in this process. Detailed spectra of Fe 2p was shown in Fig. 4f. The binding energies of 709.05 and 711.83 eV (FeOOH and FeO) [33]. All observations suggest a binding mechanism between Pb(II)/Cd(II) and the Mg-doped Fh-HA.

The change of adsorption performance during reuse of Mg-doped Fh-HA is also an index to investigate whether it can be widely used. The adsorption/desorption of Pb(II) and Cd(II) ions were carried out to investigate the reusability of Mg-doped Fh-HA. In a typical experiment, Mg-doped Fh-HA of 50 mg were added to 30 mL 170 mg/L Pb(II) and 30 mL 68 mg/L Cd(II) ion solution, then the mixture was shaken at a thermostatic shaker for 12 h. Afterwards, the residual concentration of Pb(II) and Cd(II) ions in suspension were determined by a flame atomic absorption spectrometry instrument. The residual Mg-doped Fh-HA were desorbed with 0.2, 0.5 and 1.0 mol/L HCl, HNO_3, H_2SO_4 and $CaCl_2$, respectively. Washed by deionized water for several times. Figs. S5a and b (Supporting information) showed the desorption effect of different desorption agents. Figs. S5a and b showed that 1.0 mol/L $CaCl_2$ had a much higher desorption rate when it is used as eluent than other eluent. Therefore, 1.0 mol/L $CaCl_2$ was selected as the desorption agent for Pb(II) and Cd(II) ions. The desorbed Mg-doped Fh-HA was freeze-dried and continued to be used as an adsorbent for Pb(II) and Cd(II) ions under the same conditions. The adsorption/desorption process was conducted for 3 cycles. The effect of reuse on Mg-doped Fh-HA adsorption of Pb(II) and Cd(II) ions is shown in Fig. S5c (Supporting information).

The experimental results demonstrated that Mg-doped Fh-HA has a great adsorption effect on Pb(II) and Cd(II). This sorption was better described by Langmuir model and *pseudo*-second-order model. The experimental conclusions are summarized as follows: (1) Optimal conditions for material preparation: Mg/Fe (mole ratio) = 0.2, C/Fe (mole ratio) = 2. (2) Optimum adsorption conditions: pH 6, 25 °C, the adsorption time is about 12 h, had the largest adsorption capacity of 71.43 mg/g and 27.77 mg/g for Pb(II) and Cd(II), respectively. (3) The XRD analysis showed that compared with Fh-HA, Mg-doped Fh-HA does not reduce the adsorption sites. (4) The FTIR and XPS analysis demonstrated that the presence of Pb(II) and Cd(II) in Mg-doped Fh-HA after adsorption, verifying the adsorption of Pb(II) and Cd(II) by Mg-doped Fh-HA. (5) It is further shown that the adsorption mechanism of Mg-doped Fh-HA for Pb(II) and Cd(II) is surface adsorption, mainly due to the role of the surface functional groups of Mg-doped Fh-HA. The results contribute to understanding the effects of ferrihydrite and humic acid on the transport of Pb(II) and Cd(II) in water environment. Some limitations of this study that are the complexity of water pollution and the variability of actual environmental conditions are not fully taken into account. Nevertheless, the results of the study have made an important contribution to the research of oneself and others.

Declaration of competing interest

The authors report no declarations of interest.

Acknowledgments

This work was funded by the Natural Science Foundation of China (Nos. 41771341 and 51978319), Outstanding Youth Foundation of Gansu Province (No. 20JR10RA651) and Natural Science Foundation of Gansu Province (Nos. 20JR5RA242 and 20JR10RA635). We wish to thank the Electron Microscopy Centre of Lanzhou University for the microscopy and microanalysis of our specimens.

Appendix A. Supplementary data

Supplementary material related to this article can be found, in the online version, at doi:https://doi.org/10.1016/j.cclet.2021.03.086.

References

[1] K. Fukumoto, I. Karai, S. Horiguchi, Occup. Environ. Med. 40 (1983) 220–223.
[2] H.E. Hutchison, J.M. Stark, J. Clin. Pathol. 14 (1961) 548–549.
[3] X. Liu, G. Tian, D. Jiang, et al., Environ. Sci. Poll. Res. Interface 23 (2016) 1–12.
[4] J.L. Jambor, J.E. Dutrizac, Chem. Rev. 98 (2010) 2549–2586.
[5] C.M. Hansel, S.G. Benner, S. Fendorf, Environ. Sci. Technol. 39 (2005) 7147–7153.
[6] J.N. Wang, A.M. Li, Y. Zhou, et al., Chin. Chem. Lett. 20 (2009) 1478–1482.
[7] J. Lehmann, M. Kleber, Nature 528 (2015) 60–68.
[8] B.L. Zhang, W. Qiu, P.P. Wang, et al., Chem. Eng. J. 385 (2019) 123507.
[9] C.Z. Man, Q. Zhou, Z. Yang, et al., Chin. Chem. Lett. 23 (2012) 1267–1270.
[10] Z. Xue, N. Liu, H. Hu, et al., Roy. Soc. Open Sci. 6 (2019) 182195.
[11] K. Eusterhues, T. Rennert, H. Knicker, et al., Environ. Sci. Technol. 45 (2011) 527–533.
[12] K. Kaiser, G. Guggenberger, Org. Geochem. 31 (2000) 711–725.
[13] S. Yu, L. Zhai, Y. Wang, et al., J. Environ. Chem. Eng. 3 (2015) 752–762.
[14] A. Philippe, G.E. Schaumann, Environ. Sci. Technol. 48 (2014) 8946–8962.
[15] W. Zhang, S. Mao, H. Chen, et al., Bioresour. Technol. 147 (2013) 545–552.
[16] C.M. Chen, J.J. Dynes, J. Wang, D.L. Sparks, Environ. Sci. Technol. 23 (2014) 13751–13759.
[17] Q.W. Zhou, B.H. Liao, L.N. Lin, W.W. Qiu, Z.G. Song, Sci. Total Environ. 615 (2018) 115–122.
[18] H.H. Du, C.L. Peacock, W.L. Chen, Q.Y. Huang, Chemosphere 207 (2018) 404–412.
[19] C.H. Xu, S.Y. Shi, X.Q. Wang, et al., J. Hazard. Mater. 381 (2019) 120974.
[20] N. Liu, L.F. Shi, X.H. Han, et al., Chin. Chem. Lett. 31 (2020) 386–390.
[21] H.Y. Zhan, Y.T. Wang, X.Y. Mi, et al., Chin. Chem. Lett. 31 (2020) 2843–2848.
[22] S. Goldberg, J. Colloids Interface Sci. 285 (2005) 509–517.
[23] A. Terracciano, J. Zhang, C. Christodoulatos, et al., J. Environ. Sci. 57 (2017) 8–14.
[24] W. Qiao, P. Zhang, L. Sun, et al., Chin. Chem. Lett. 31 (2020) 2742–2746.
[25] Y. Li, M.Q. Li, J. Zhang, X.Y. Xu, Chin. Chem. Lett. 3 (2019) 762–766.
[26] W. Qiao, P. Zhang, L. Sun, et al., Chin. Chem. Lett. 31 (2020) 2742–2746.
[27] J. Liang, X. Li, Z. Yu, et al., ACS Sustain. Chem. Eng. 5 (2017) 5040–5048.
[28] Z. Liu, D. Tian, F. Shen, et al., Chin. Chem. Lett. 30 (2019) 2221–2224.
[29] Y. Qiu, Q. Zhang, M. Li, et al., Water Air Soil Pollut. 230 (2019) 84–95.
[30] Lalhmunsiama, P.L. Gupta, J. Hyunhoon, et al., J. Taiwan Inst. Chem. Eng. 71 (2017) 206–213.
[31] M.A. Islam, S. Sabar, A. Benhouria, et al., J. Taiwan Inst. Chem. Eng. 74 (2017) 96–104.
[32] L. Zhang, J. Guo, X. Huang, et al., RSC Adv. 9 (2019) 365–376.
[33] Q. Zhou, B. Liao, L. Lin, et al., Sci. Total Environ. 615 (2018) 115–122.